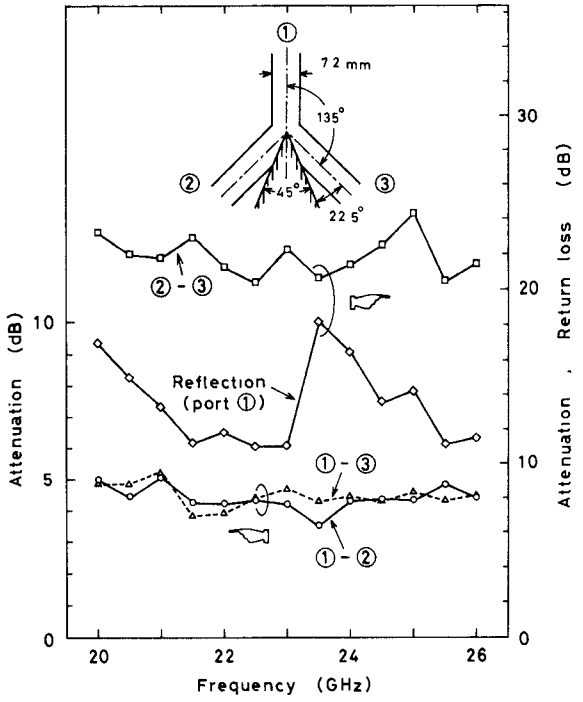

Fig. 5. Measured performance of the Y-junction-type power divider with the reflector.

Fig. 5 shows the measured performance of the Y-junction-type power divider with the reflector. The top view of the structure is shown in the inset in Fig. 5. In this example, the waveguide axes of output ports are inclined at 45° to that of the input port. The vertex of the wedge is located at the intersection of the three waveguide axes, and each face of the wedge is placed at 22.5° with the output waveguide. The average power division is 4.42 dB, and the isolation is greater than 20 dB. Although the isolation is improved, the power division is not improved unexpectedly. The performance of this type of power divider depends on the angle between output waveguides. It seems that the power divider with small output angle exhibits good performance. The reason why the power division was not improved has not been made clear at the present stage. The reflection characteristics at the input port are also shown in Fig. 5. The cause of the difference between experimental and ideal power divisions is considered to be due to the radiation, since the reflection is small (return loss >10 dB).

IV. Conclusion

The corners and power dividers with the metallic reflector have been fabricated from the rectangular dielectric image line and have been tested in the 20–26-GHz range. It is found that the bending loss of the corner with the reflector is comparable to that of the curved waveguide of large bending radius. The proposed Y-function-type power divider exhibits good performance. The metallic reflector can be applied to other passive components for dielectric waveguide millimeter-wave integrated circuits.

References

[1] T. Itoh, "Dielectric waveguide-type millimeter-wave integrated circuits," *Infrared and Millimeter Waves*, vol. 4, K. J. Button and J. C. Wiltse, Ed. New York: Academic Press, 1981, ch. 5.

[2] R. M. Knox, "Dielectric waveguide microwave integrated circuits—An overview," *IEEE Trans. Microwave Theory Tech.*, vol. MTT-24, pp. 806–814, Nov 1976

[3] T. Tamir, *Integrated Optics*. Berlin: Springer-Verlag, 1975

[4] D. D. King, "Properties of dielectric image lines," *IRE Trans. Microwave Theory Tech.*, vol. MTT-3, pp. 75–81, Mar. 1955.

[5] K. Solbach, "The measurement of the radiation losses in dielectric image line bends and the calculation of a minimum acceptable curvature radius," *IEEE Trans. Microwave Theory Tech.*, vol. MTT-27, pp. 51–53, Jan. 1979.

[6] W. Schlosser and H. G. Unger, "Partially filled waveguides and surface waveguides of rectangular cross section," *Advances in Microwaves*, vol. 1, L. Young, Ed. New York: Academic Press, 1966, pp. 319–387.

Broadside-Coupled Slot-Line Field Components

RAINEE NAVIN SIMONS, MEMBER, IEEE

Abstract—**This paper presents expressions for the odd- and even-mode electric field components and also the magnetic field components in the air, overlay, and dielectric regions of the broadside-coupled slot-line structure. These expressions are numerically computed, and the fields in the cross section and the longitudinal section are illustrated. The surface current distribution on the metal surfaces are also illustrated.**

I. Introduction

The slot-line on a dielectric substrate [1] is a very useful transmission line for realizing nonreciprocal MIC components [2]–[5]. Recently, Cohn [6] has presented the electric and magnetic field components in the dielectric and air regions of a single slot-line. Besides, Simons and Arora [7] have presented expressions for the odd- and even-mode electric field components and the magnetic field components in the air and dielectric regions of an edge-coupled slot-line.

In this paper, expressions for the odd- and even-mode electric field components, and also the magnetic field components in the dielectric and air regions of a suspended broadside-coupled slot-line with an overlay [8], are presented. The dielectric substrate and the overlays are assumed to be isotropic and homogeneous and are of arbitrary thickness and relative permittivity. The conducting cover and the zero-thickness metallization on the substrate are assumed to have infinite conductivity. These expressions are numerically computed at various points in the dielectric region and the air regions of the structure. The odd- and even-mode electric field, the magnetic field in the cross section, and the odd- and even-mode magnetic field in the longitudinal section through the slot are illustrated. Besides, the current distribution on the metal surfaces and the magnetic field tangential to the metal surfaces are illustrated. Finally, a slot-line with a lower ground plane is considered. The current paths on the lower ground plane and the magnetic field tangential to the lower ground plane are illustrated.

II. Derivation of the Field Components

The suspended broadside-coupled slot-line with an overlay is illustrated in Fig. 1(a). For the case of even excitation, a magnetic wall is placed along the plane of symmetry. It then suffices to restrict the analysis to the upper half of the structure (Fig. 1(b)). A similar simplification is possible for the case of odd excitation, except that the magnetic wall at the plane of symmetry is replaced by an electric wall (Fig. 1(b)). As in the earlier analysis

Manuscript received March 23, 1983; revised August 3, 1983.

R. N. Simons is with the Centre for Applied Research in Electronics (CARE), Indian Institue of Technology Delhi, Hauz Khas, New Delhi-110016, India.

0018-9480/84/0100-0116$01.00 ©1984 IEEE

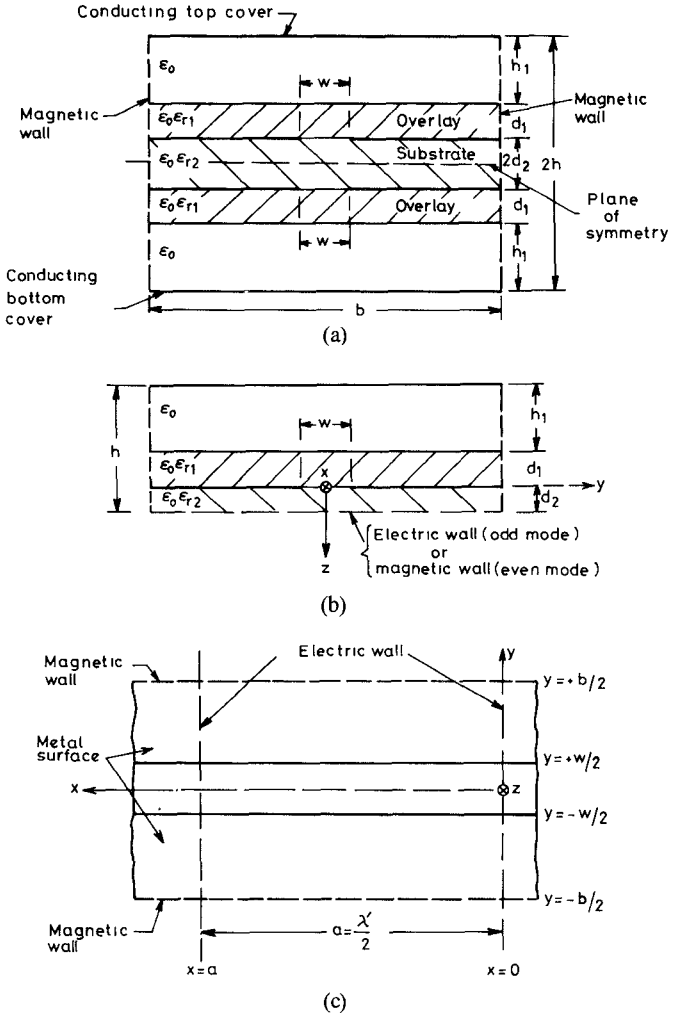

Fig. 1. (a) Schematic of the suspended broadside-coupled slot-line with overlay. (b) Development of waveguide model for field components: An electric wall is placed at the plane $z = d_2$ for the odd-mode of excitation; and the electric wall is replaced by a magnetic wall for the even-mode of excitation. (c) Insertion of transverse electric walls at $x = 0$ and $x = a$.

[8], the broadside-coupled slot-line problem is reduced to a rectangular wavegiude problem by inserting electric walls in the planes perpendicular to the slot at $x = 0$ and $x = a = \lambda'/2$ (λ' is the slot-mode wavelength) and magnetic wall at $y = \pm b/2$, and this is illustrated in Fig. 1(c).

On the substrate side of the slot ($0 \leqslant z \leqslant d_2$), the E_y and E_z components of the electric field and the H_x, H_y, H_z components of the magnetic field exist. From Maxwell's equations it follows that the E_x component of the electric field on the substrate side of the slot is zero. On the overlay side of the slot ($-d_1 \leqslant z \leqslant 0$), all components of the electric field exist. The E_y component of the electric field and the H_x component of the magnetic field are determined as explained in an earlier analysis [8], while the rest of the electric field and the magnetic field components are determined by the application of Maxwell's equations as explained in [9]. At this point it should be noted that the H_x and H_z components of the magnetic field on the overlay side of the slot are similar to those presented by Cohn [6] for the case of a single slot-line.

The rectangular coordinates x, y, z, slot width w, substrate of relative permittivity ϵ_{r2} and thickness $2d_2$, overlays of relative permittivity ϵ_{r1} and thickness d_1, and the height h_1 of the conducting cover above the overlays are indicated in Fig. 1(a). A factor $\exp j(\omega t - 2\pi x/\lambda')$ is assumed for each field component, implying wave propagation in the $+x$ direction only. V_0 is the voltage directly across the slot and is given by

$$V_0 = \int_{-w/2}^{+w/2} E_y\, dy. \tag{1}$$

III. Odd-Mode Field Components

A. Substrate Side of the Slot, $0 \leqslant z \leqslant d_2$

$$E_y = \frac{2V_0}{b} \sum_{n=\frac{1}{2},\frac{3}{2},\cdots}^{\infty} \frac{\sin n\pi\delta}{n\pi\delta} \cos\frac{2\pi ny}{b} \cdot \{\cosh\gamma_{n2}z - \coth\gamma_{n2}d_2 \sinh\gamma_{n2}z\} \tag{2}$$

$$E_z = -\frac{2V_0}{b} \sum_{n=\frac{1}{2},\frac{3}{2},\cdots}^{\infty} \frac{1}{F_{n2}} \frac{\sin n\pi\delta}{n\pi\delta} \sin\frac{2\pi ny}{b} \cdot \{\coth\gamma_{n2}d_2 \cosh\gamma_{n2}z - \sinh\gamma_{n2}z\} \tag{3}$$

$$H_x = j\frac{2V_0}{\eta b}\left(\frac{\lambda}{\lambda'}\right)^2\left(\frac{b}{\lambda}\right)\left[1-\epsilon_{r2}\left(\frac{\lambda'}{\lambda}\right)^2\right] \sum_{n=\frac{1}{2},\frac{3}{2},\cdots}^{\infty} \frac{1}{nF_{n2}} \frac{\sin n\pi\delta}{n\pi\delta} \cdot \cos\frac{2\pi ny}{b} \{\coth\gamma_{n2}d_2 \cosh\gamma_{n2}z - \sinh\gamma_{n2}z\} \tag{4}$$

$$H_y = \frac{2V_0}{\eta b}\frac{\lambda}{\lambda'} \sum_{n=\frac{1}{2},\frac{3}{2},\cdots}^{\infty} \frac{1}{F_{n2}} \frac{\sin n\pi\delta}{n\pi\delta} \sin\frac{2\pi ny}{b} \cdot \{\coth\gamma_{n2}d_2 \cosh\gamma_{n2}z - \sinh\gamma_{n2}z\} \tag{5}$$

$$H_z = \frac{2V_0}{\eta_b}\frac{\lambda}{\lambda'} \sum_{n=\frac{1}{2},\frac{3}{2},\cdots}^{\infty} \frac{\sin n\pi\delta}{n\pi\delta} \cos\frac{2\pi ny}{b}, \cdot \{\cosh\gamma_{n2}z - \coth\gamma_{n2}d_2 \sinh\gamma_{n2}z\}. \tag{6}$$

B. Overlay Side of the Slot, $-d_1 \leqslant z \leqslant 0$

$$E_x = -j\frac{2V_0}{\lambda'} \sum_{n=\frac{1}{2},\frac{3}{2},\cdots}^{\infty} \frac{1}{n\left[1+(b/n\lambda')^2\right]} \frac{\sin n\pi\delta}{n\pi\delta} \sin\frac{2\pi ny}{b} \cdot \{\coth q_n - \tanh r_n\} \sinh\gamma_{n1}|z| \tag{7}$$

$$E_y = \frac{2V_0}{b} \sum_{n=\frac{1}{2},\frac{3}{2},\cdots}^{\infty} \frac{\sin n\pi\delta}{n\pi\delta} \cos\frac{2\pi ny}{b} \cdot \left\{\cosh\gamma_{n1}|z| - \left[\frac{\tanh r_n + (b/n\lambda')\coth q_n}{1+(b/n\lambda')^2}\right]\sinh\gamma_{n1}|z|\right\} \tag{8}$$

$$E_z = \frac{2V_0}{b} \sum_{n=\frac{1}{2},\frac{3}{2},\cdots}^{\infty} \frac{1}{F_{n1}} \frac{\sin n\pi\delta}{n\pi\delta} \sin\frac{2\pi ny}{b} \cdot \{\sinh\gamma_{n1}|z| - \tanh r_n \cosh\gamma_{n1}|z|\} \tag{9}$$

$$H_x = j\frac{2V_0}{\eta b}\left(\frac{\lambda}{\lambda'}\right)^2\frac{b}{\lambda} \sum_{n=\frac{1}{2},\frac{3}{2},\cdots}^{\infty} \frac{1}{nF_{n1}} \frac{\sin n\pi\delta}{n\pi\delta} \cos\frac{2\pi ny}{b} \cdot \left\{\left[\frac{F_{n1}^2 \coth q_n - \epsilon_r(\lambda'/\lambda)^2 \tanh r_n}{1+(b/n\lambda')^2}\right]\cosh\gamma_{n1}|z| - \left[1-\epsilon_r(\lambda'/\lambda)^2\right]\sinh\gamma_{n1}|z|\right\} \tag{10}$$

$$H_y = \frac{2V_0}{\eta b}\frac{\lambda}{\lambda'}\sum_{n=\frac{1}{2},\frac{3}{2},\cdots}^{\infty}\frac{1}{F_{n1}}\frac{\sin n\pi\delta}{n\pi\delta}\sin\frac{2\pi ny}{b}$$

$$\cdot\left\{\left[\frac{F_{n1}^2\coth q_n + \epsilon_r(b/n\lambda)^2\tanh r_n}{1+(b/n\lambda')^2}\right]\cosh\gamma_{n1}|z| - \sinh\gamma_{n1}|z|\right\} \quad (11)$$

$$H_z = \frac{2V_0}{\eta b}\frac{\lambda}{\lambda'}\sum_{n=\frac{1}{2},\frac{3}{2},\cdots}^{\infty}\frac{\sin n\pi\delta}{n\pi\delta}\cos\frac{2\pi ny}{b}$$

$$\cdot[\cosh\gamma_{n1}|z| - \coth q_n\sinh\gamma_{n1}|z|]. \quad (12)$$

C. Air Region Above the Overlay, $-(d_1+h_1)\leqslant z\leqslant -d_1$

The expressions for the field components in the air region above the overlay are derived from (7)–(12) by replacing $\gamma_{n1}|z|$ with $\gamma_{n1}|-d_1|$. Further, the expression for E_x, E_y, and H_z are multiplied by the factor

$$\frac{\sinh\gamma_n(-|z|+d_1+h_1)}{\sinh\gamma_n h_1}$$

and the expressions for E_z, H_x, and H_y are multiplied by the factor

$$\frac{\cosh\gamma_n(-|z|+d_1+h_1)}{\cosh\gamma_n h_1}.$$

This is done in order to satisfy the boundary conditions at the overlay–air interface and also on the conducting cover. Symbols not defined above are $\eta = 376.7\ \Omega$, $p = \lambda/\lambda'$, $\delta = w/b$, and

$$v = \sqrt{(\lambda/\lambda')^2 - 1}, \quad F_n = \frac{b\gamma_n}{2\pi n} = \sqrt{1+\left(\frac{bv}{2anp}\right)^2} \quad (13)$$

$$u_1 = \sqrt{\epsilon_{r1} - (\lambda/\lambda')^2}, \quad F_{n1} = \frac{b\gamma_{n1}}{2\pi n} = \sqrt{1-\left(\frac{bu_1}{2anp}\right)^2} \quad (14)$$

$$u_2 = \sqrt{\epsilon_{r2} - (\lambda/\lambda')^2}, \quad F_{n2} = \frac{b\gamma_{n2}}{2\pi n} = \sqrt{1-\left(\frac{bu_2}{2anp}\right)^2} \quad (15)$$

$$r_n = \frac{2\pi nF_{n1}d_1}{b} + \tanh^{-1}\left[\frac{F_{n1}}{F_n\epsilon_{r1}}\coth\frac{2\pi nF_nh_1}{b}\right] \quad (16)$$

$$q_n = \frac{2\pi nF_{n1}d_1}{b} + \coth^{-1}\left[\frac{F_n}{F_{n1}}\coth\frac{2\pi nF_nh_1}{b}\right]. \quad (17)$$

IV. Even-Mode Field Components

A. Substrate Side of the Slot, $0\leqslant z\leqslant d_2$

The expressions for the field components on the substrate side of the slot are derived from (2)–(6) by replacing $\coth\gamma_{n1}d_2$ with $\tanh\gamma_{n1}d_2$.

B. Overlay Side of the Slot, $-d_1\leqslant z\leqslant 0$

The expressions for the field components on the overlay side of the slot are the same as (7)–(12).

C. Air Region Above the Overlay, $-(d_1+h_1)\leqslant z\leqslant -d_1$

The expressions for the field components in the air region are the same as those derived previously for the odd-excitation. Further, (13)–(17) are also valid for the case of even-excitation.

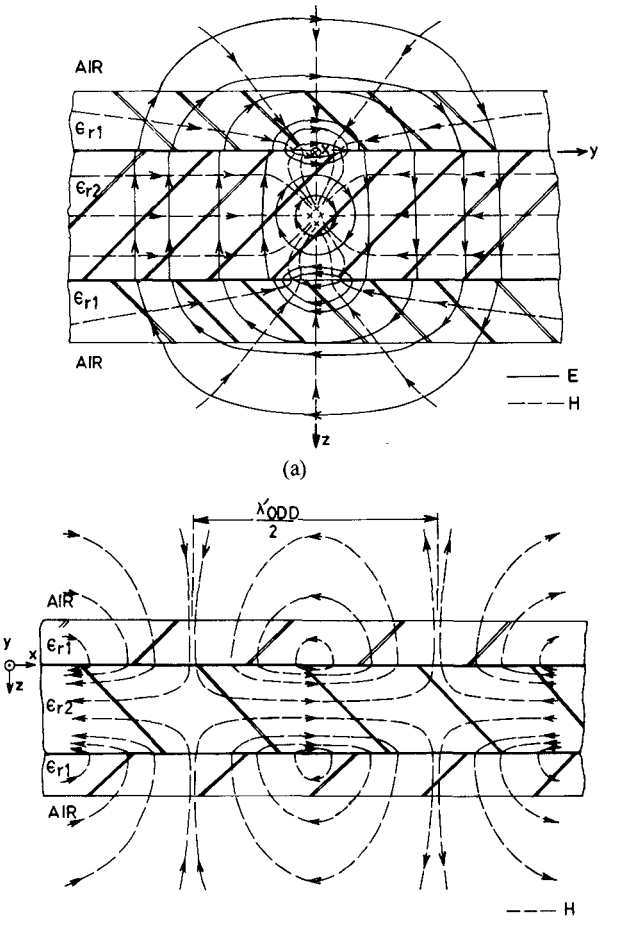

Fig. 2. (a) Electric field and magnetic field distribution in the cross section ($x = 0$ plane) for the odd-mode. (b) Magnetic field in the longitudinal section ($y = 0$ plane) through the slot for the odd-mode.

V. Numerical Results

When carrying out the computations, ϵ_{r1} was set equal to $\epsilon_{r2} = 9.8$, $d_1 = d_2 = 0.025$ in, $w = 0.02$ in, $h = 0.5$ in, $b = 2$ in, and frequency was set equal to 15 GHz. At 15 GHz, the above structure also supports higher order modes. However, the computations and the figures presented here illustrate the fields pertaining to the dominant mode only. Since the expressions involve summing an infinite series, the following criterion for terminating the series at n_t was adopted: $n_t = n_0/(1+z/z_1)$, where n_0 and z_1 are constants. In the above case, $n_0 = 1000$ and $z_1 = 0.005$ in were found suitable. Hence, 1000 terms were used at $z = 0$, and 10 terms at $z = 0.5$ in.

The computed electric field and the magnetic field in the transverse section for the odd-mode of excitation are illustrated in Fig. 2(a). The electric field in the overlays and in the air regions extend across the slots. However, in the substrate (that is, in the region below the slots), they form concentric circles. With increasing distance from the center, these circles at first warp and finally split into segments. These segments extend across the slots as well as bridge the upper and lower metal surfaces. Although this was not indicated in [8, fig. 2(c)], it makes no difference in the analysis. The magnetic field lines passing through the center of the slot lie in a plane normal to the slot. The magnetic field lines passing through points away from the center of the slot towards the edges of the conductor warp into curved surfaces.

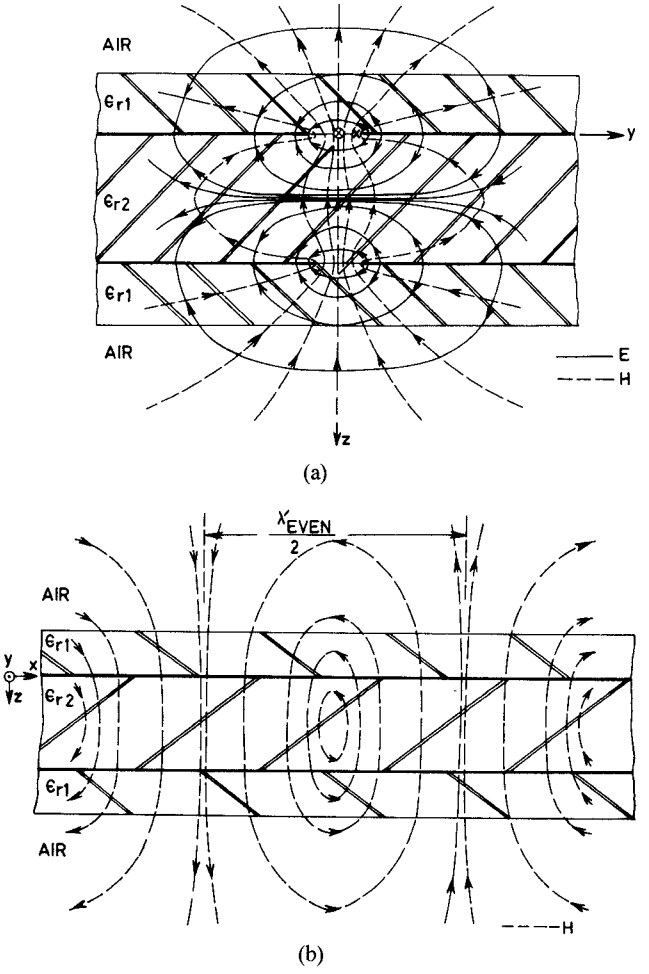

Fig. 3. (a) Electric field and magnetic field distribution in the cross section ($x = 0$ plane) for the even-mode. (b) Magnetic field in the longitudinal section ($y = 0$ plane) through the slot for the even-mode

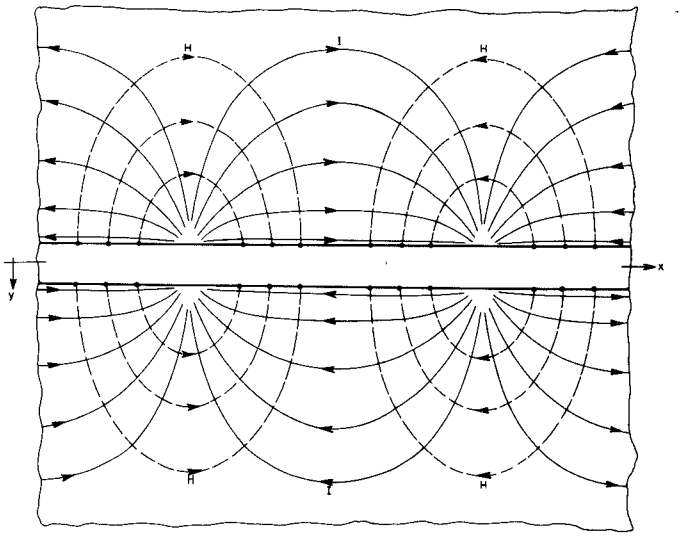

Fig. 4. The current distribution on the metallization and also the magnetic field tangential to the metallization for the even-mode.

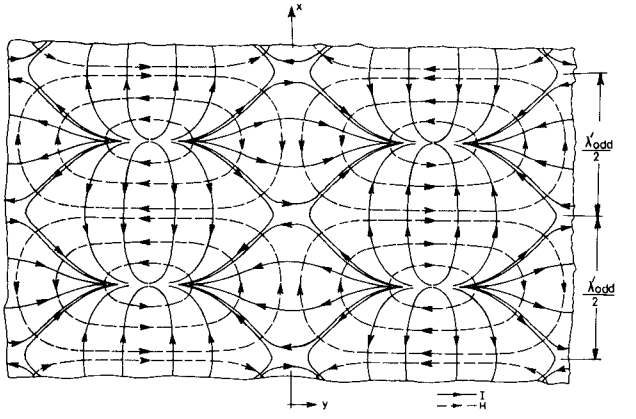

Fig. 5. The upper half of the broadside-coupled slot-line for the odd-mode of excitation is considered as a slot-line with a lower ground plane. The current distribution on the lower ground plane, and also the magnetic field tangential to the lower ground plane, is illustrated.

This effect is more predominant in the overlay side of the slot. However, in the substrate (that is, in the region below the slots), the magnetic field lines are radially distributed about the center. In the region away from the slot that is much greater than the slot width, the magnetic field lines are parallel to the metal surfaces. The longitudinal view in Fig. 2(b) shows that in the overlays (and also in the air regions) the magnetic field lines curve and return to the slot at half-wavelength intervals. Consequently, a wave propagating along the structure has an elliptically polarized magnetic field.

Fig. 3(a) illustrates the computed electric field and the magnetic field in the transverse section for the even-mode of excitation. The electric field lines extend across the slot in the air regions, overlays, and in the substrate. The magnetic field distribution in the air regions and the overlays is observed to be similar to the case of odd-excitation. In the substrate, the magnetic field lines are continuous everywhere. Hence, the slots are coupled by the magnetic field. The longitudinal view in Fig. 3(b) shows that the magnetic field lines curve and return to the slots at half-wavelength intervals. Hence, a propagating wave has an elliptically polarized magnetic field for even-excitation, also.

Fig. 4 illustrates the computed current paths on the metal surfaces for the even-mode of excitation. The figure also illustrates the magnetic field lines tangential to the conducting surface. The surface current density is observed to be the greatest at the edges of the slot and decreases with distance away from the slot. Further, the magnetic field is elliptically polarized in this plane, also. The computed current paths on the conducting surfaces for the odd-mode of excitation is similar to Fig. 4 and, hence, is not presented.

Finally, it is observed that the broadside-coupled slot-line for the odd-mode of excitation reduces to a slot-line with a lower ground plane [10]. Fig. 5 illustrates the computed current paths on the lower ground plane and also the tangential magnetic field.

VI. Suggested Applications

The elliptically polarized magnetic field in the longitudinal section can be successfully exploited in the design of slot-line four-port circulators [5] and latching ferrite differential phase-shifter [2]. The externally applied dc magnetic field should be parallel to the plane of the substrate and perpendicular to the length of the slot.

The elliptically polarized magnetic field in the plane containing the slot can be successfully exploited in the design of slot-line three-port circulators [3]. The externally applied dc magnetic field should be perpendicular to the plane containing the slot.

A knowledge of the field components should also prove useful in the design of mode launchers, such as between microstrip and slot-line [5], [16], and between coplanar waveguide (CPW) and slot-line [11].

Besides, it should also prove useful in the study of coupling between a slot-line and a cylindrical dielectric resonator. Goebel and Schieblich [12] have studied the coupling between a slot-line and a cylindrical dielectric resonator. Their studies show that the coupling is efficient when the slot runs tangential to the resonator and when the edges of the resonator extend into the slot. Such a study should also prove useful in filter applications [13].

Finally, a knowledge of the current distribution on the metal surfaces should prove useful in the design of slot-line antennas [10], [14], [15]. The lower ground plane, besides being useful in slot-line antennas, can also act as a heat sink in applications involving solid-state devices.

VII. Conclusion

The paper presents expressions for the odd- and even-mode electric field components and the magnetic field components in the air and dielectric regions of broadside-coupled slot-lines. These expressions have been numerically evaluated and the fields in the cross section and the longitudinal section are illustrated. Besides, the computed current paths on the metal surfaces and the tangential magnetic field are illustrated. The magnetic field in the longitudinal section, and in the plane of the slot, is elliptically polarized.

Acknowledgment

The author wishes to thank L. A. Robinson of Stanford Research Institute and S. B. Cohn of S. B. Cohn Associates for providing the necessary references. The author is also grateful to S. B. Cohn for several helpful communications on slot-line. The author is also grateful to the reviewers for their helpful comments.

References

[1] S. B. Cohn, "Slot-line on a dielectric substrate," *IEEE Trans. Microwave Theory Tech.*, vol. MTT-17, pp. 768–778, Oct 1969.
[2] G H. Robinson and J. L. Allen, "Slot-line application to miniature ferrite devices," *IEEE Trans Microwave Theory Tech.*, vol MTT-17, pp. 1097–1101, Dec. 1969.
[3] N. Ogasawara and M. Kaji, "Coplanar-guide and slot-guide junction circulators," *Electron. Lett.*, vol. 7, pp 220–221, May 1971.
[4] M. De Vecchis, L. Raczy, and P. Gelin, "A new slot-line broadband isolator," in *Proc. 3rd Eur Microwave Conf.*, vol. 2, B.9.6, Sept. 4–7, 1973.
[5] L. Courtois and M. De Vecchis, "A new class of nonreciprocal components using slot-line," *IEEE Trans. Microwave Theory Tech.*, vol. MTT-23, pp. 511–516, June 1975.
[6] S. B. Cohn, "Slot-line field components," *IEEE Trans. Microwave Theory Tech.*, vol. MTT-20, pp. 172–174, Feb. 1972.
[7] R. N. Simons and R. K. Arora, "Coupled slot-line field components," *IEEE Trans. Microwave Theory Tech.*, vol. MTT-30, pp. 1094–1099, July 1982.
[8] R. N. Simons, "Suspended broadside coupled slotline with overlay," *IEEE Trans. Microwave Theory Tech.*, vol. MTT-30, pp. 76–81, Jan. 1982.
[9] R. N. Simons, "Studies on microwave slot-line and integrated fin-line," Ph.D. thesis, Dept. Electrical Eng., Indian Institute of Technology Delhi, New Delhi, India, 1982.
[10] J. W. Greiser, "Coplanar stripline antenna," *Microwave J.*, vol 19, pp. 47–49, Oct. 1976.
[11] M. Houdart and C. Aury, "Various excitations of coplanar waveguide," in *IEEE MTT-S Int. Microwave Symp. Dig.*, April 30–May 2, 1979, pp. 116–118.
[12] U. Goebel and C. Schieblish, "Broadband fin-line circulators," in *IEEE MTT-S Int. Microwave Symp. Dig.*, June 14–19, 1982, pp. 249–251.
[13] J. K. Plourde and C. L. Ren, "Application of dielectric resonators in microwave components," *IEEE Trans. Microwave Theory Tech.*, vol. MTT-29, pp. 754–770, Aug. 1981.
[14] S. N. Prasad and S. Mahapatra, "A novel MIC slot-line antenna," in *Proc. 9th Eur. Microwave Conf.*, Sept. 17–21, 1979, pp. 120–124.
[15] P. A. R. Holder, "*X*-band microwave integrated circuits using slotline and coplanar waveguide," *Radio Electron. Eng.*, vol. 48, pp. 38–42, Jan./Feb 1978.
[16] J. B. Knorr, "Slot-line transitions," *IEEE Trans. Microwave Theory Tech.*, vol. MTT-22, pp. 548–554, May 1974.

Radar-Echo Location of Conducting Spheres in Waveguide

P. I. SOMLO, SENIOR MEMBER, IEEE

Abstract—**The radar-echo locations of conducting spheres placed in the center of the broad wall of a rectangular guide were measured using the synthetic-pulse technique. The measuring instrument was a six-port reflectometer whose results in the frequency domain were transformed digitally into the time domain. It was found that, as the size of the spheres was reduced, the radar-echo locations approached the center of the spheres in an oscillatory manner. The findings are somewhat unexpected, as the echo centers for some sphere sizes appear to be farther away from the source than their physical centers.**

I. Introduction

It has been reported that conducting spheres placed in waveguides have the special property that their reflection coefficients are quasi-constant with frequency [1]. It has also been shown empirically that this is true for all sphere sizes, with diameters nearly up to guide height. The magnitude of the reflection coefficient $|\Gamma|$ of a small sphere varies as the volume of the sphere. This finding has been confirmed theoretically using a perturbation method [2].

Because conducting spheres produce a quasi-constant magnitude of reflection coefficient and may easily be positioned in a waveguide, they are useful as special tuning elements which offer wide-band compensation. $\text{Arg}(\Gamma)$ may be adjusted by axial positioning, and $|\Gamma|$ by lateral positioning. Steel balls (bearing balls) may be moved and held in place by small external magnets. In the Locating Reflectometer [3], for instance, the directivities of both the reference and the measuring directional couplers were increased over the whole *X*-band by placing small spheres near the start of the multi-hole coupling region. It has been shown [3, fig. 9] how the internal reflections of a horn antenna were reduced to a negligible level over the whole *X*-band by suitably positioning (and gluing) four steel balls near the throat of a horn antenna.

The purpose of this investigation was to measure the effective locations of conducting spheres placed in the center of the broad wall of rectangular waveguide. One may define a number of ball-position criteria. One such definition may be position of a lumped susceptance producing the same $|\Gamma|$ as a ball. This definition is physically inexact, since the larger balls cannot be regarded as lumped obstacles. A similar definition would be to use $\arg(\Gamma)$. Another definition regards the balls to be positioned where $\text{Re}\,\Gamma(t) = 0$, since the ball is assumed loss-free. Again, this

Manuscript received April 4, 1983; revised August 16, 1983.
The author is with CSIRO, Division of Applied Physics, P.O. Box 218, Lindfield, NSW 2070, Australia